

Interplay of pseudo-Hermitian symmetries and degenerate manifolds in the eigenspectrum of non-Hermitian systems

Grigory A. Starkov¹

¹*Institute for Theoretical Physics and Astrophysics,
University of Würzburg, D-97074 Würzburg, Germany**

(Dated: February 13, 2024)

In this letter, we study how the spectrum of pseudo-Hermitian systems is influenced by the ambiguity in the choice of the pseudo-metric operator. In particular, we analyze the case when different parameter-independent choices of pseudo-metric are possible and how it can lead to the appearance of robust degenerate manifolds in the parameter space of the system.

Introduction.— Recent years show an increased interest in the study of non-Hermitian phenomena. Non-Hermitian Hamiltonians arise ubiquitously as the effective description of open systems [1] and generally in many-body interacting systems [2–14], where the system itself acts as a thermalizing bath for its constituents. One of their most captivating features is the occurrence of the special type of degeneracies called Exceptional Points (*EPs*), where the coalescence of several eigenvalues is accompanied also by the simultaneous coalescence of the corresponding eigenvectors. The applications of *EPs* include increasing sensitivity of quantum sensors [15–19], mode switching in waveguides [20–23] and optical microcavities [24–26], state conversion [27, 28] and laser emission management [29, 30], to name a few. Despite promising practical properties, the realization of *EPs* is complicated by the necessity of tuning a system to the spectral vicinity of a required *EP*. Nevertheless, the number of fine-tuning parameters can be lowered in the presence of symmetries. As such, investigation of the influence of the symmetries on the eigenspectrum of a non-Hermitian system is of immense practical interest. In this regards, a widely considered class of symmetries is that of anti-Unitary symmetries [31–34], which all can be related either to \mathcal{PT} -symmetry or to pseudo-Hermiticity [31]. In addition to that, \mathcal{PT} -symmetric systems are known to be pseudo-Hermitian [1, 35–39], therefore we focus exclusively on the latter property.

A system is said to be pseudo-Hermitian when its Hamiltonian satisfies

$$\hat{\zeta}\hat{H}\hat{\zeta}^{-1} = \hat{H}^\dagger, \quad (1)$$

where $\hat{\zeta}$ is an invertible Hermitian operator called pseudo-metric. The eigenvalues of a pseudo-Hermitian Hamiltonian can be either real or form complex conjugated pairs, and *EPs* separate the corresponding parameter regions. In general, the pseudo-metric is not uniquely defined [40, 41] and may depend on the parameters of the system [35–38, 42–45], however, in a lot of relevant situations, one can choose it to be parameter-independent [46–50]. In the latter case, in the parameter regions with real eigenvalues, the levels can be uniquely characterized by the topological indices ± 1 , which govern the formation

of *EPs* [51–55]: Second-order *EPs*, where two levels coalesce, are provided only by the level pairs with opposite indices. The structure of higher-order *EPs* is restricted insofar they can be obtained from several second-order *EPs* tuned to coalesce.

Notably the parameter-independent choice of the pseudo-metric can itself be non-unique, which enables one to define the set of topological indices with respect to either of the pseudo-metrics. Taking into account the interplay between different sets of indices is important to predict the formation of *EPs*. For example, a second-order *EPs* is realized only when it is allowed by all sets of topological indices. Moreover, such interplay can influence even normal non-defective degeneracies (also called diabolical points) which are present in non-Hermitian systems as well. The symmetry stabilization of the diabolical points has been studied recently in Refs. [56, 57]. Here, we discuss a completely new mechanism for such stabilization: formation of a second-order *EP* can be allowed by one set of indices and forbidden by another one; in this case, a non-defective crossing of two levels is promoted to a robust degenerate manifold in the parameter space.

Pseudo-metric and the structure of eigenvectors. — Away from *EPs*, the Hamiltonian has a complete biorthonormal basis of right and left eigenvectors [1, 38]:

$$\hat{H}(\vec{p})|R_n(\vec{p})\rangle = \varepsilon(\vec{p})|R_n(\vec{p})\rangle, \quad (2)$$

$$\langle L_n(\vec{p})|\hat{H}(\vec{p}) = \varepsilon_n(\vec{p})\langle L_n(\vec{p})|, \quad (3)$$

$$\langle L_n(\vec{p})|R_{n'}(\vec{p})\rangle = \delta_{n,n'}. \quad (4)$$

We focus on the levels corresponding to the real eigenvalues. In this case, the pseudo-metric is known to bijectively map the right eigensubspace onto the left one. For a level corresponding to a non-degenerate eigenvalue, it implies

$$\hat{\zeta}|R_n(\vec{p})\rangle = c_n(\vec{p})|L_n(\vec{p})\rangle. \quad (5)$$

For a degenerate eigenvalue, Eq. (5) still holds provided we choose the right eigenvectors to diagonalize $\langle R_m|\hat{\zeta}|R_n\rangle$.

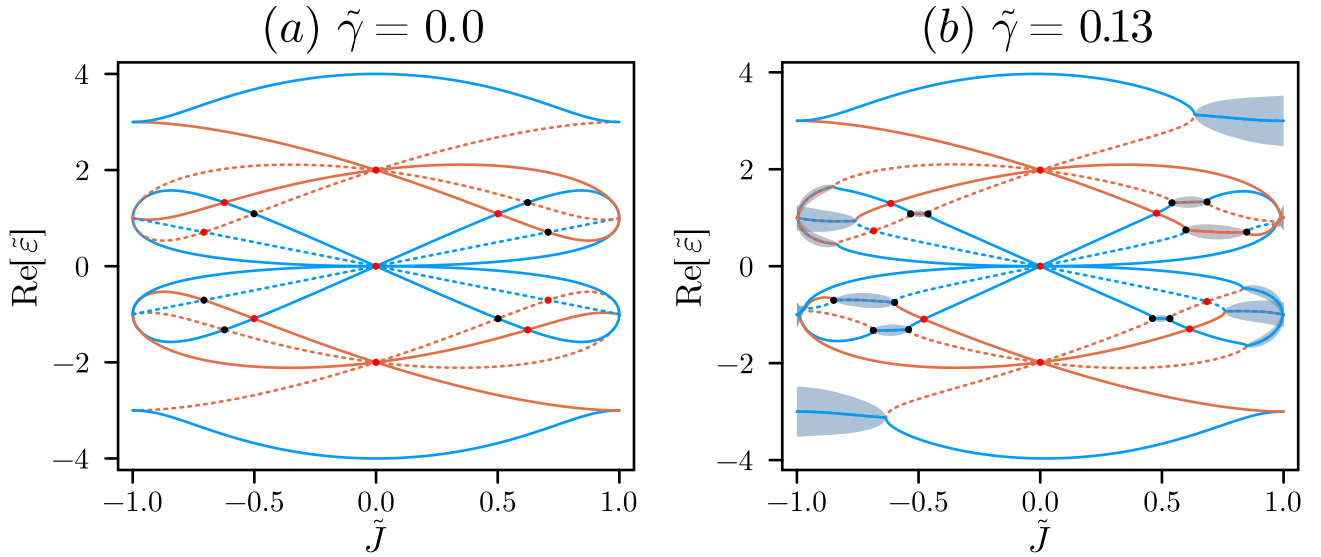


FIG. 1: Eigenspectrum of the non-Hermitian transverse-field Ising chain in the case of longitudinal gain (loss). The panels plot the real parts of the normalized eigenenergies $\text{Re}[\tilde{\varepsilon}]$ while the imaginary parts are displayed as shaded ribbons with the width proportional to $\text{Im}[\tilde{\varepsilon}]$. The solid (dashed) linestyle denotes the $\zeta_{\mathcal{P}} = +1$ ($\zeta_{\mathcal{P}} = -1$) topological index with respect to the first choice of the pseudo-metric operator. The blue (orange) color denotes the $\eta = +1$ ($\eta = -1$) topological index with respect to the second choice of the pseudo-metric operator. Diabolical points protected by the combination of two pseudo-metric operators (red dots) are stable. In comparison, the crossings of the levels that are allowed to form second-order EPs by all the choices of pseudo-metric operator (black dots in panel (a)) naturally split into pairs of second-order EPs (pairs of black dots in panel (b)) as soon as gain (loss) is turned on.

The biorthonormality condition (4) does not completely fix the normalization of the left and right eigenvectors. We can use it to rescale both eigenvectors in such a way, as to remove $c_n(\vec{p})$ almost completely with the exception of its sign:

$$\hat{\zeta}|R_n(\vec{p})\rangle = \zeta_n|L_n(\vec{p})\rangle, \quad (6)$$

$$\zeta_n = \text{sign} \left[\sqrt{\langle R_n(\vec{p}) | \hat{\zeta} | R_n(\vec{p}) \rangle} \right] = \pm 1. \quad (7)$$

The scalar product inside the sign turns zero only at the EPs [1, 51]. Therefore, the topological index ζ_n of the specific level is conserved in the whole parameter region where the corresponding eigenvalue stays real [51].

If there is more than one parameter-independent pseudo-metric operator, than one can define the topological indices with respect to either of them. There is, however, an important caveat, that the right choice of the right and left eigenvectors satisfying Eq. (5) could be different for different pseudo-metric operators. However, this problem can only arise for the left and right eigenvectors corresponding to a degenerate eigenvalue.

Effective projected Hamiltonian in the vicinity of a degeneracy. — In the vicinity of a second-order degeneracy, be it defective or non-defective, we can project onto the states involved. We can use then the identity (7) to restrict the structure of the projected Hamiltonian.

Let the vector of parameters \vec{p}' correspond to a non-degenerate point in the vicinity of a second-order degeneracy, where the two levels involved have real eigenenergies. We can linearize the Hamiltonian around \vec{p}' ,

$$\hat{H}(\vec{p}' + \Delta\vec{p}) = \hat{H}(\vec{p}') + \vec{\nabla}\hat{H}(\vec{p}') \cdot \Delta\vec{p}, \quad (8)$$

and then project it onto the left $\langle L_i(\vec{p}') |$ and right $|R_i(\vec{p}')\rangle$ eigenvectors $i = 1, 2$ corresponding to the degeneracy. Assuming that the eigenvectors are rescaled to make Eq. (7) true, one can easily prove [51] that the matrix elements of the projected Hamiltonian satisfy

$$\langle L_i(\vec{p}') | \hat{H}(\vec{p}') | R_j(\vec{p}') \rangle = \zeta_i \zeta_j \overline{\langle L_j(\vec{p}') | \hat{H}(\vec{p}') | R_i(\vec{p}') \rangle}, \quad (9)$$

where the bar on top denotes the complex conjugation. This identity restricts the structure of the projected Hamiltonian to

$$H_{i,j}^P = \langle L_i(\vec{p}') | \hat{H}(\vec{p}') | R_j(\vec{p}') \rangle = \begin{pmatrix} \varepsilon_1(\vec{p}') + \vec{u}_1(\vec{p}') \cdot \Delta\vec{p} & \vec{w}(\vec{p}') \cdot \Delta\vec{p} \\ \zeta_1 \zeta_2 \vec{w}^*(\vec{p}') \cdot \Delta\vec{p} & \varepsilon_2(\vec{p}') + \vec{u}_2(\vec{p}') \cdot \Delta\vec{p} \end{pmatrix}, \quad (10)$$

where \vec{u}_1 and \vec{u}_2 are real-valued. As one can clearly see, the projected Hamiltonian can have a non-Hermitian form only if $\zeta_1 \zeta_2 = -1$, which means that the second-order EPs are formed only by levels with opposite topological indices.

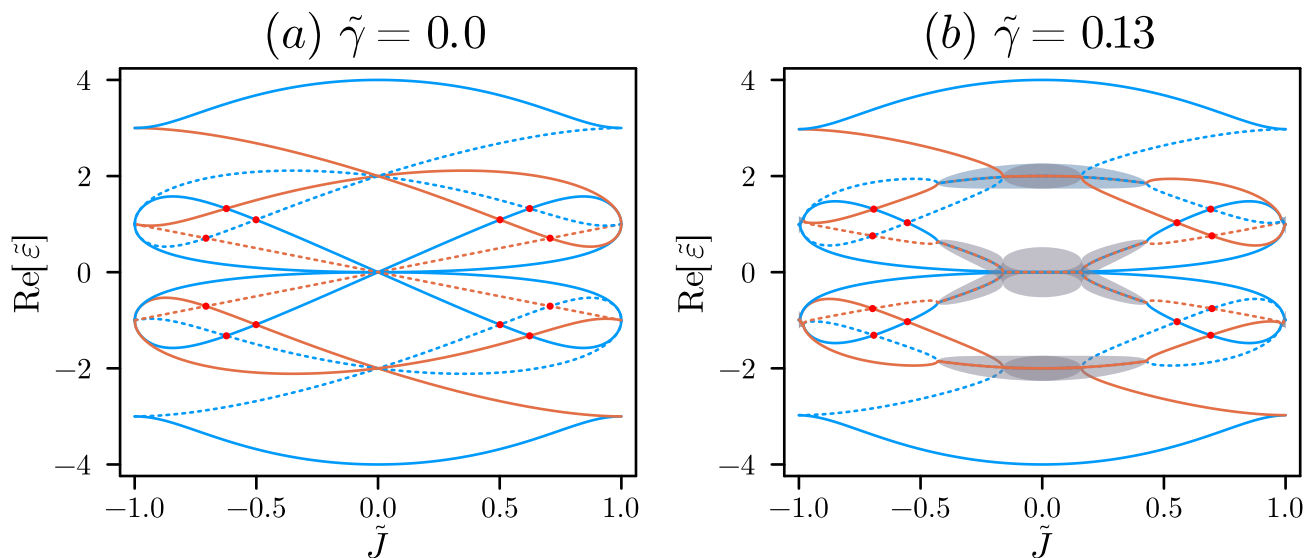


FIG. 2: Eigenspectrum of the non-Hermitian transverse-field Ising model in the case of transversal gain (loss). The panels plot the real parts of the normalized eigenenergies $\text{Re}[\tilde{\epsilon}]$ while the imaginary parts are displayed as shaded ribbons with the width proportional to $\text{Im}[\tilde{\epsilon}]$. The solid (dashed) linestyle denotes the $\zeta_{\mathcal{P}} = +1$ ($\zeta_{\mathcal{P}} = -1$) topological index with respect to the first choice of the pseudo-metric operator. The blue (orange) color denotes the $\eta = +1$ ($\eta = -1$) topological index with respect to the second choice of the pseudo-metric operator. Diabolical points protected by the combination of two pseudo-metric operators (red dots) are stable.

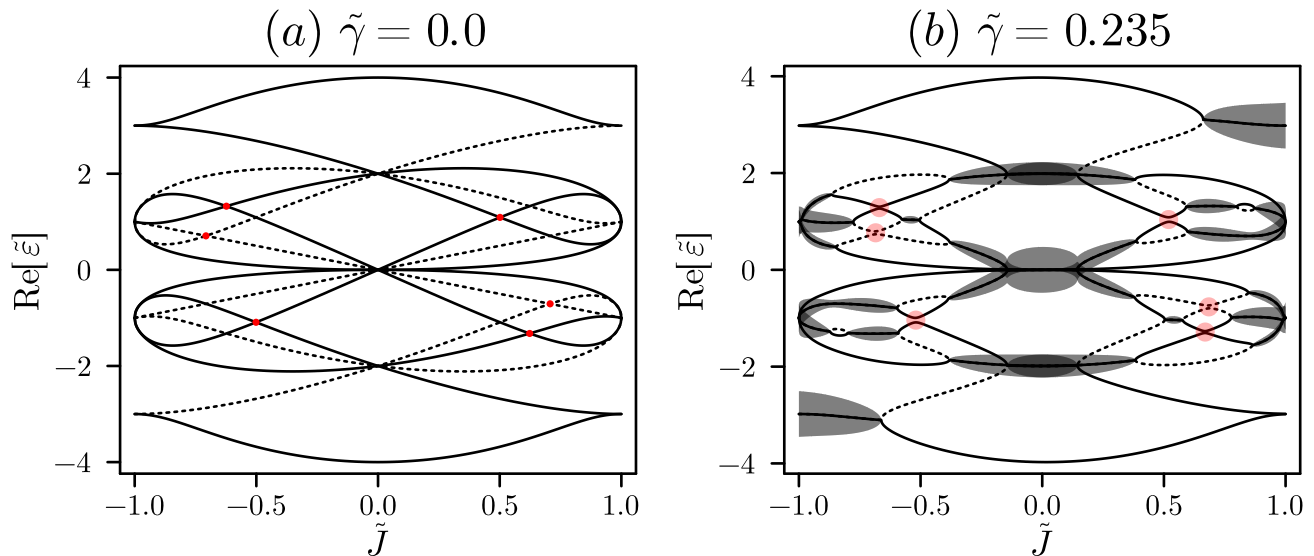


FIG. 3: Eigenspectrum of the non-Hermitian transverse-field Ising model in the case of mixed longitudinal-transversal gain (loss). The panels plot the real parts of the normalized eigenenergies $\text{Re}[\tilde{\epsilon}]$ while the imaginary parts are displayed as shaded ribbons with the width proportional to $\text{Im}[\tilde{\epsilon}]$. There is only one parameter-independent choice of the pseudo-metric operator and the corresponding topological indices are denoted by solid ($\zeta_{\mathcal{P}} = +1$) or dashed ($\zeta_{\mathcal{P}} = -1$) linestyle. Turning on gain (loss) transforms the same parity diabolical points (red dots in panel (a)) into avoided crossings (red shaded areas in panel (b)).

Let us assume now, that we have another choice of the pseudo-metric operator $\hat{\eta}$, which defines a compatible set of topological indices. We can repeat the same steps to derive the projected Hamiltonian in the basis of eigenvectors that satisfies Eq. (7) for this second operator.

The new eigenvectors $\langle \tilde{L}_i(\vec{p}') |$ and $|\tilde{R}_i(\vec{p}')\rangle$ are related to the old ones by a simple rescaling that preserves the biorthonormality (4):

$$|\tilde{R}_i(\vec{p}')\rangle = \alpha_i |R_i(\vec{p}')\rangle, \quad \langle \tilde{L}_i(\vec{p}') | = \frac{1}{\alpha_i} \langle L_i(\vec{p}') |. \quad (11)$$

The projected Hamiltonian in the new basis is

$$\begin{aligned} \tilde{H}_{i,j}^P &= \langle \tilde{L}_i(\vec{p}') | \hat{H}(\vec{p}') | \tilde{R}_j(\vec{p}') \rangle = \\ &= \begin{pmatrix} \varepsilon_1(\vec{p}') + \vec{u}_1(\vec{p}') \cdot \Delta\vec{p} & \vec{w}(\vec{p}') \cdot \Delta\vec{p} \\ \eta_1 \eta_2 \vec{w}^*(\vec{p}') \cdot \Delta\vec{p} & \varepsilon_2(\vec{p}') + \vec{u}_2(\vec{p}') \cdot \Delta\vec{p} \end{pmatrix}. \end{aligned} \quad (12)$$

The two forms of the projected Hamiltonian (12) and (10) should lead to the same eigenspectrum, i.e., they are similar matrices with identical characteristic polynomials. This means that the products of off-diagonal elements, equal up to a sign to the free term of the characteristic polynomial, should be the same for two matrices:

$$\zeta_1 \zeta_2 |\vec{w}(\vec{p}') \cdot \Delta\vec{p}|^2 = \eta_1 \eta_2 |\vec{w}(\vec{p}') \cdot \Delta\vec{p}|^2. \quad (13)$$

If now

$$\zeta_1 \zeta_2 = -\eta_1 \eta_2, \quad (14)$$

then the off-diagonal matrix element is forced to be zero in either of the bases: $\vec{w}(\vec{p}') = \vec{w}(\vec{p}') = 0$.

Robust degenerate manifold. — Let us now choose the expansion point \vec{p}' corresponding to a second-order diabolical point, i.e. second order non-defective degeneracy. If the indices of the two levels satisfy Eq. (14), we can rewrite the projected Hamiltonian (10) as

$$H^P = [\varepsilon(\vec{p}') + \vec{u}_+ \cdot \Delta\vec{p}] \mathbb{1} + (\vec{u}_- \cdot \Delta\vec{p}) \sigma_z. \quad (15)$$

Here, $\mathbb{1}$ and σ_z are the identity and the z Pauli 2×2 matrices. The vectors \vec{u}_\pm are symmetric and antisymmetric combinations of $\vec{u}_{1,2}$:

$$\vec{u}_\pm = \frac{\vec{u}_1 \pm \vec{u}_2}{2}. \quad (16)$$

The equation $\vec{u}_- \cdot \Delta\vec{p} = 0$ defines then locally a manifold of diabolical points. This manifold is robust in the sense that it must naturally appear as long as the dimensionality of the parameter space ≥ 2 . Although the condition (14) prevents the two levels either from opening the gap or from forming an *EP* between each other, one of the levels can still form an *EP* with some third level. As such, the degenerate manifold of diabolical points is bounded by the manifolds of Exceptional Points.

In comparison, if $\zeta_1 \zeta_2 = \eta_1 \eta_2$, then generally \vec{w} is non-zero and is not collinear with \vec{u}_- . As a result, any non-zero $\Delta\vec{p}$ opens the gap, which is either real ($\zeta_1 \zeta_2 = 1$) or imaginary ($\zeta_1 \zeta_2 = -1$).

Examples. — We choose our examples from the class of \mathcal{PT} -symmetric \mathcal{P} -pseudo-Hermitian extensions of the transverse-field Ising model.

$$\hat{H} = \hat{H}_0 + \hat{H}_{\text{nh}}, \quad (17)$$

$$\hat{H}_0 = \sum_{j=1}^N \Delta \hat{\sigma}_j^x - J \sum_{j=1}^{N-1} \hat{\sigma}_j^z \hat{\sigma}_{j+1}^z, \quad (18)$$

$$\hat{H}_{\text{nh}} = i \sum_{j=1}^N (\gamma_j^z \hat{\sigma}_j^z + \gamma_j^x \hat{\sigma}_j^x). \quad (19)$$

Single qubits effectively described by non-Hermitian Hamiltonians have already been experimentally realized in various solid state systems such as trapped ions, ultracold and Rydberg atoms [58–60], Bose–Einstein condensate [61], superconducting [62–64] or nitrogen-vacancies qubits [65]. In principle, our exemplar class of models can be obtained in experiment by engineering the coupling between several such effective non-Hermitian qubits by coupling them, for example, to a lossless resonator [66].

We define the parity and the time reversal operators as the mirror flip of the chain and the complex conjugation respectively [48, 50, 51]:

$$\hat{\mathcal{P}} \sigma_j^s \hat{\mathcal{P}}^{-1} = \sigma_{N+1-j}^s, \quad \hat{\mathcal{T}} i \hat{\mathcal{T}}^{-1} = -i. \quad (20)$$

The \mathcal{PT} -symmetry of the model requires that

$$\gamma_j^z = -\gamma_{N+1-j}^z, \quad \gamma_j^x = -\gamma_{N+1-j}^x. \quad (21)$$

In addition to \mathcal{PT} -symmetric, the model is also pseudo-Hermitian with $\hat{\zeta} = \hat{\mathcal{P}}$. The Hermitian part \hat{H}_0 of the model is integrable and can be diagonalized via a combination of Jordan-Wigner and generalized Bogolyubov transformations [67]. As such, one can compute the topological indices $\zeta_{\mathcal{P}}$ corresponding to $\hat{\mathcal{P}}$ analytically, which has already been done in Ref. [51].

We consider three specific arrangements of gain (loss) coefficients $\{\gamma_j^z, \gamma_j^x\}$.

- Purely longitudinal gain (loss): $\gamma_j^x \equiv 0$. In this case, there is a second choice of pseudo-metric operator $\hat{\eta} = \hat{\mathcal{U}}$, where

$$\hat{\mathcal{U}} = \otimes_{j=1}^N \hat{\sigma}_j^x. \quad (22)$$

The corresponding topological indices are $\eta = \zeta_{\mathcal{U}} = -1^{n_{fm}}$, where n_{fm} is the number of excited Bogolyubov fermionic modes. Note that the eigenspectrum is generally non-degenerate, so the corresponding topological indices are compatible.

- Purely transversal gain (loss): $\gamma_j^z \equiv 0$. In this case, $\hat{\mathcal{U}}$ commutes with \hat{H} , and there is a second choice of the pseudo-metric operator $\hat{\eta} = \hat{\mathcal{P}} \hat{\mathcal{U}}$. The corresponding topological indices are $\eta = \zeta_{\mathcal{P}} \zeta_{\mathcal{U}}$.
- Mixed gain (loss): $\gamma_j^z, \gamma_j^x \neq 0$. In this case, the symmetry is lowered, and there is no second choice of the pseudo-metric operator.

Dissipative dynamics described by a non-Hermitian Hamiltonian can be interpreted as a consequence of continuous measurements combined with the post-selection on measurement results [62]. In this context, tuning the combination of the gain (loss) parameters (γ_i^x, γ_i^z) can be physically interpreted as changing the direction of the effective magnetic field used to probe the qubit i .

For concreteness, we assume $N = 4$ and staggered gain (loss): $\gamma_j^z = \gamma \times (-1)^{j-1}$ in the purely longitudinal case,

$\gamma_j^x = \gamma \times (-1)^{j-1}$ in the purely transversal case, and $\gamma_j^x = \gamma_j^z = 0.5\gamma \times (-1)^{j-1}$. Using numerical diagonalization, we obtain the eigenspectra in each of the cases and plot them in Figs. 1, 2 and 3 respectively. There, we display the real parts of the normalized eigenvalues $\tilde{\varepsilon} = \varepsilon/\sqrt{J^2 + \Delta^2}$ as the functions of the normalized Ising coupling $\tilde{J} = J/\sqrt{J^2 + \Delta^2}$ for different fixed values of normalized gain (loss) strength $\tilde{\gamma} = \gamma/\sqrt{J^2 + \Delta^2}$. In all of the figures, the imaginary parts of the eigenvalues are visualized as the shaded ribbons; the solid (dashed) linestyle denotes $\zeta = 1$ ($\zeta = -1$). In Figs. 1 and 2, the blue (orange) color of the lines denotes $\zeta = 1$ ($\zeta = -1$).

In Figs. 1 (longitudinal case) and 2 (transversal case), we single out the crossings, where the levels have same indices with respect to one pseudo-metric, and opposite indices with respect to another one. According to the results of the previous section, these crossings form degeneracy lines in the two-dimensional parameter space $(\tilde{J}, \tilde{\gamma})$. As we change $\tilde{\gamma}$, such crossings do not open the gap and just shift in \tilde{J} , i.e. they are robust with the respect to the dissipation. At larger $\tilde{\gamma}$, a degeneracy line ends at a second-order *EP*, formed by one of the crossing levels with some third level.

In Fig. 3, we single out the same parity crossings. Since there is no symmetry protection anymore, these crossings naturally open the gaps as soon as gain (loss) is turned on.

Conclusions. — In this letter, we have focused on non-Hermitian systems with pseudo-Hermitian symmetry and studied the interplay of different parameter-independent choices of the pseudo-metric operator. We have shown it to be important both for the defective and non-defective degeneracies. Formation of a second-order *EP* between a pair of levels is possible only if it is allowed with respect to all pseudo-metric operators. Moreover, if the formation of a second-order *EP* between two levels is allowed for one choice of the pseudo-metric but forbidden for another one, the crossing of such levels has to be non-defective and is promoted to a whole manifold of non-defective degeneracies.

The results presented here are completely general and do not depend on the physical nature of the system realizing the non-Hermitian Hamiltonian as long as it has the symmetry properties we discussed. As such, the results can be also applied to the non-Hermitian Bloch Hamiltonians arising in topological band theory [68, 69] or to the effective non-Hermitian Hamiltonians arising in interacting many-body contexts [5–14].

Acknowledgements. — I would like to thank prof. Björn Trauzettel for the fruitful and encouraging discussions. This work was supported by the Würzburg-Dresden Cluster of Excellence ct.qmat, EXC2147, project-id 390858490.

* grigori.starkov@uni-wuerzburg.de

- [1] Y. Ashida, Z. Gong, and M. Ueda, Non-hermitian physics, *Advances in Physics* **69**, 249 (2020).
- [2] A. A. Zyuzin and A. Y. Zyuzin, Flat band in disorder-driven non-hermitian weyl semimetals, *Phys. Rev. B* **97**, 041203 (2018).
- [3] M. Papaaj, H. Isobe, and L. Fu, Nodal arc of disordered dirac fermions and non-hermitian band theory, *Phys. Rev. B* **99**, 201107 (2019).
- [4] B. Michen, T. Micallo, and J. C. Budich, Exceptional non-hermitian phases in disordered quantum wires, *Phys. Rev. B* **104**, 035413 (2021).
- [5] V. Kozii and L. Fu, Non-hermitian topological theory of finite-lifetime quasiparticles: Prediction of bulk fermi arc due to exceptional point (2017), [arXiv:1708.05841 \[cond-mat.mes-hall\]](https://arxiv.org/abs/1708.05841).
- [6] T. Yoshida, R. Peters, and N. Kawakami, Non-hermitian perspective of the band structure in heavy-fermion systems, *Phys. Rev. B* **98**, 035141 (2018).
- [7] K. Kimura, T. Yoshida, and N. Kawakami, Chiral-symmetry protected exceptional torus in correlated nodal-line semimetals, *Phys. Rev. B* **100**, 115124 (2019).
- [8] T. Yoshida, R. Peters, N. Kawakami, and Y. Hatsugai, Exceptional band touching for strongly correlated systems in equilibrium, *Progress of Theoretical and Experimental Physics* **2020**, 12A109 (2020), <https://academic.oup.com/ptep/article-pdf/2020/12/12A109/35415188/ptaa059.pdf>.
- [9] Y. Nagai, Y. Qi, H. Isobe, V. Kozii, and L. Fu, Dmft reveals the non-hermitian topology and fermi arcs in heavy-fermion systems, *Phys. Rev. Lett.* **125**, 227204 (2020).
- [10] Y. Michishita, T. Yoshida, and R. Peters, Relationship between exceptional points and the kondo effect in *f*-electron materials, *Phys. Rev. B* **101**, 085122 (2020).
- [11] R. Rausch, R. Peters, and T. Yoshida, Exceptional points in the one-dimensional hubbard model, *New Journal of Physics* **23**, 013011 (2021).
- [12] C. Lehmann, M. Schüler, and J. C. Budich, Dynamically induced exceptional phases in quenched interacting semimetals, *Phys. Rev. Lett.* **127**, 106601 (2021).
- [13] L. Crippa, J. C. Budich, and G. Sangiovanni, Fourth-order exceptional points in correlated quantum many-body systems, *Phys. Rev. B* **104**, L121109 (2021).
- [14] M. Reitner, L. Crippa, D. R. Fus, J. C. Budich, A. Toschi, and G. Sangiovanni, Protection of correlation-induced phase instabilities by exceptional susceptibilities (2023), [arXiv:2307.00849 \[cond-mat.str-el\]](https://arxiv.org/abs/2307.00849).
- [15] J. Wiersig, Enhancing the sensitivity of frequency and energy splitting detection by using exceptional points: Application to microcavity sensors for single-particle detection, *Phys. Rev. Lett.* **112**, 203901 (2014).
- [16] J. Wiersig, Sensors operating at exceptional points: General theory, *Phys. Rev. A* **93**, 033809 (2016).
- [17] W. Chen, Ş. K. Özdemir, G. Zhao, J. Wiersig, and L. Yang, Exceptional points enhance sensing in an optical microcavity, *Nature* **548**, 192 (2017).
- [18] H. Hodaei, A. U. Hassan, S. Wittek, H. Garcia-Gracia, R. El-Ganainy, D. N. Christodoulides, and M. Khajavikhan, Enhanced sensitivity at higher-order exceptional points, *Nature* **548**, 187 (2017).
- [19] M. P. Hokmabadi, A. Schumer, D. N. Christodoulides,

- and M. Khajavikhan, Non-hermitian ring laser gyroscopes with enhanced sagnac sensitivity, *Nature* **576**, 70 (2019).
- [20] S. N. Ghosh and Y. D. Chong, Exceptional points and asymmetric mode conversion in quasi-guided dual-mode optical waveguides, *Scientific Reports* **6**, 10.1038/srep19837 (2016).
- [21] J. Doppler, A. A. Mailybaev, J. Böhm, U. Kuhl, A. Girschik, F. Libisch, T. J. Milburn, P. Rabl, N. Moiseyev, and S. Rotter, Dynamically encircling an exceptional point for asymmetric mode switching, *Nature* **537**, 76 (2016).
- [22] X.-L. Zhang, S. Wang, B. Hou, and C. T. Chan, Dynamically encircling exceptional points: In situ control of encircling loops and the role of the starting point, *Phys. Rev. X* **8**, 021066 (2018).
- [23] A. Laha, A. Biswas, and S. Ghosh, Nonadiabatic modal dynamics around exceptional points in an all-lossy dual-mode optical waveguide: Toward chirality-driven asymmetric mode conversion, *Phys. Rev. Appl.* **10**, 054008 (2018).
- [24] A. Laha and S. Ghosh, Connected hidden singularities and toward successive state flipping in degenerate optical microcavities, *Journal of the Optical Society of America B* **34**, 238 (2017).
- [25] A. Laha, A. Biswas, and S. Ghosh, Next-nearest-neighbor resonance coupling and exceptional singularities in degenerate optical microcavities, *Journal of the Optical Society of America B* **34**, 2050 (2017).
- [26] A. Laha, A. Biswas, and S. Ghosh, Minimally asymmetric state conversion around exceptional singularities in a specialty optical microcavity, *Journal of Optics* **21**, 025201 (2019).
- [27] A. Laha, D. Beniwal, S. Dey, A. Biswas, and S. Ghosh, Third-order exceptional point and successive switching among three states in an optical microcavity, *Phys. Rev. A* **101**, 063829 (2020).
- [28] A. Laha, D. Beniwal, and S. Ghosh, Successive switching among four states in a gain-loss-assisted optical microcavity hosting exceptional points up to order four, *Phys. Rev. A* **103**, 023526 (2021).
- [29] M. Brandstetter, M. Liertzer, C. Deutsch, P. Klang, J. Schöberl, H. E. Türeci, G. Strasser, K. Unterrainer, and S. Rotter, Reversing the pump dependence of a laser at an exceptional point, *Nature Communications* **5**, 10.1038/ncomms5034 (2014).
- [30] Z. J. Wong, Y.-L. Xu, J. Kim, K. O'Brien, Y. Wang, L. Feng, and X. Zhang, Lasing and anti-lasing in a single cavity, *Nature Photonics* **10**, 796 (2016).
- [31] P. Delplace, T. Yoshida, and Y. Hatsugai, Symmetry-protected multifold exceptional points and their topological characterization, *Phys. Rev. Lett.* **127**, 186602 (2021).
- [32] M. Stålhammar and E. J. Bergholtz, Classification of exceptional nodal topologies protected by \mathcal{PT} symmetry, *Phys. Rev. B* **104**, L201104 (2021).
- [33] S. Sayyad and F. K. Kunst, Realizing exceptional points of any order in the presence of symmetry, *Phys. Rev. Res.* **4**, 023130 (2022).
- [34] S. Sayyad, M. Stalhammar, L. Rodland, and F. K. Kunst, Symmetry-protected exceptional and nodal points in non-hermitian systems (2022), [arXiv:2204.13945 \[quant-ph\]](https://arxiv.org/abs/2204.13945).
- [35] A. Mostafazadeh, Pseudo-Hermiticity versus PT symmetry: The necessary condition for the reality of the spectrum of a non-Hermitian Hamiltonian, *Journal of Mathematical Physics* **43**, 205 (2002).
- [36] A. Mostafazadeh, Pseudo-Hermiticity versus PT-symmetry. II. A complete characterization of non-Hermitian Hamiltonians with a real spectrum, *Journal of Mathematical Physics* **43**, 2814 (2002).
- [37] A. Mostafazadeh, Pseudo-Hermiticity versus PT-symmetry III: Equivalence of pseudo-Hermiticity and the presence of antilinear symmetries, *Journal of Mathematical Physics* **43**, 3944 (2002).
- [38] A. Mostafazadeh, Pseudo-Hermitian Representation of Quantum Mechanics, *International Journal of Geometric Methods in Modern Physics* **07**, 1191 (2010).
- [39] R. Zhang, H. Qin, and J. Xiao, PT-symmetry entails pseudo-hermiticity regardless of diagonalizability, *Journal of Mathematical Physics* **61**, 012101 (2020).
- [40] Z. Bian, L. Xiao, K. Wang, X. Zhan, F. A. Onanga, F. Ruzicka, W. Yi, Y. N. Joglekar, and P. Xue, Conserved quantities in parity-time symmetric systems, *Phys. Rev. Res.* **2**, 022039 (2020).
- [41] K. S. Agarwal, J. Muldoon, and Y. N. Joglekar, Conserved quantities in non-hermitian systems via vectorization method, *Acta Polytechnica* **62**, 1–7 (2022).
- [42] J. Gong and Q. hai Wang, Time-dependent \mathcal{PT} -symmetric quantum mechanics, *Journal of Physics A: Mathematical and Theoretical* **46**, 485302 (2013).
- [43] S. Deffner and A. Saxena, Jarzynski equality in \mathcal{PT} -symmetric quantum mechanics, *Phys. Rev. Lett.* **114**, 150601 (2015).
- [44] D.-J. Zhang, Q.-h. Wang, and J. Gong, Quantum geometric tensor in \mathcal{PT} -symmetric quantum mechanics, *Phys. Rev. A* **99**, 042104 (2019).
- [45] D.-J. Zhang, Q.-h. Wang, and J. Gong, Time-dependent \mathcal{PT} -symmetric quantum mechanics in generic non-hermitian systems, *Phys. Rev. A* **100**, 062121 (2019).
- [46] C. M. Bender and S. Boettcher, Real spectra in non-hermitian hamiltonians having \mathcal{PT} symmetry, *Phys. Rev. Lett.* **80**, 5243 (1998).
- [47] C. E. Rüter, K. G. Makris, R. El-Ganainy, D. N. Christodoulides, M. Segev, and D. Kip, Observation of parity-time symmetry in optics, *Nature Physics* **6**, 192 (2010).
- [48] C. Li, G. Zhang, X. Z. Zhang, and Z. Song, Conventional quantum phase transition driven by a complex parameter in a non-hermitian \mathcal{PT} -symmetric ising model, *Phys. Rev. A* **90**, 012103 (2014).
- [49] L. Tetling, M. V. Fistul, and I. M. Eremin, Linear response for pseudo-hermitian hamiltonian systems: Application to \mathcal{PT} -symmetric qubits, *Phys. Rev. B* **106**, 134511 (2022).
- [50] G. A. Starkov, M. V. Fistul, and I. M. Eremin, Quantum phase transitions in non-hermitian pt-symmetric transverse-field ising spin chains, *Annals of Physics* , 169268 (2023).
- [51] G. A. Starkov, M. V. Fistul, and I. M. Eremin, Formation of exceptional points in pseudo-hermitian systems, *Phys. Rev. A* **108**, 022206 (2023).
- [52] M. Krein, A generalization of some investigations of linear differential equations with periodic coefficients, in *Doklady Akad. Nauk SSSR*, Vol. 73 (1950) pp. 445–448.
- [53] I. M. Gel'fand and V. B. Lidskii, On the structure of the regions of stability of linear canonical systems of differen-

- tial equations with periodic coefficients, *Uspekhi Matematicheskikh Nauk* **10**, 3 (1955).
- [54] V. Starzhinskii and V. Yakubovich, *Linear differential equations with periodic coefficients 2 vol.* (Wiley London, 1975).
- [55] A. Melkani, Degeneracies and symmetry breaking in pseudo-hermitian matrices, *Phys. Rev. Res.* **5**, 023035 (2023).
- [56] H. Xue, m. Q. Wang, B. Zhang, and Y. D. Chong, Non-hermitian dirac cones, *Phys. Rev. Lett.* **124**, 236403 (2020).
- [57] S. Sayyad, Protection of all nondefective twofold degeneracies by antiunitary symmetries in non-hermitian systems, *Phys. Rev. Res.* **4**, 043213 (2022).
- [58] L. Ding, K. Shi, Q. Zhang, D. Shen, X. Zhang, and W. Zhang, Experimental determination of \mathcal{PT} -symmetric exceptional points in a single trapped ion, *Phys. Rev. Lett.* **126**, 083604 (2021).
- [59] J. A. S. Lourenço, G. Higgins, C. Zhang, M. Henrich, and T. Macrì, Non-hermitian dynamics and \mathcal{PT} -symmetry breaking in interacting mesoscopic rydberg platforms, *Phys. Rev. A* **106**, 023309 (2022).
- [60] J. Li, A. K. Harter, J. Liu, L. de Melo, Y. N. Joglekar, and L. Luo, Observation of parity-time symmetry breaking transitions in a dissipative floquet system of ultracold atoms, *Nature Communications* **10**, 10.1038/s41467-019-08596-1 (2019).
- [61] H. Cartarius and G. Wunner, Model of a \mathcal{PT} -symmetric bose-einstein condensate in a δ -function double-well potential, *Phys. Rev. A* **86**, 013612 (2012).
- [62] M. Naghiloo, M. Abbasi, Y. N. Joglekar, and K. W. Murch, Quantum state tomography across the exceptional point in a single dissipative qubit, *Nature Physics* **15**, 1232 (2019).
- [63] W. Chen, M. Abbasi, Y. N. Joglekar, and K. W. Murch, Quantum jumps in the non-hermitian dynamics of a superconducting qubit, *Phys. Rev. Lett.* **127**, 140504 (2021).
- [64] S. Dogra, A. A. Melnikov, and G. S. Paraoanu, Quantum simulation of parity-time symmetry breaking with a superconducting quantum processor, *Communications Physics* **4**, 10.1038/s42005-021-00534-2 (2021).
- [65] Y. Wu, W. Liu, J. Geng, X. Song, X. Ye, C.-K. Duan, X. Rong, and J. Du, Observation of parity-time symmetry breaking in a single-spin system, *Science* **364**, 878 (2019).
- [66] G. A. Starkov, M. V. Fistul, and I. M. Eremin, Schrieffer-wolff transformation for non-hermitian systems: application for \mathcal{PT} -symmetric circuit qed (2023), [arXiv:2309.09829 \[quant-ph\]](https://arxiv.org/abs/2309.09829).
- [67] E. Lieb, T. Schultz, and D. Mattis, Two soluble models of an antiferromagnetic chain, *Annals of Physics* **16**, 407 (1961).
- [68] H. Shen, B. Zhen, and L. Fu, Topological band theory for non-hermitian hamiltonians, *Phys. Rev. Lett.* **120**, 146402 (2018).
- [69] I. Mandal and E. J. Bergholtz, Symmetry and higher-order exceptional points, *Phys. Rev. Lett.* **127**, 186601 (2021).